Nanotechnology

PAPER • OPEN ACCESS

# Flexible planar supercapacitors by straightforward filtration and laser processing steps

To cite this article: Olli Pitkänen *et al* 2020 *Nanotechnology* **31** 495403

OPEN ACCESS
IOP Publishing
Nanotechnology

Nanotechnology **31** (2020) 495403 (8pp)
https://doi.org/10.1088/1361-6528/abb336

# Flexible planar supercapacitors by straightforward filtration and laser processing steps

**Olli Pitkänen[1], Toprak Eraslan[2], Dániel Sebők[3], Imre Szenti[3], Ákos Kukovecz[3], Robert Vajtai[2] and Krisztian Kordas[1]**

[1] Microelectronics Research Unit, Faculty of Information Technology and Electrical Engineering, University of Oulu, Oulu, Finland
[2] Department of Material Science and NanoEngineering, Rice University, Houston, Texas 77005, United States of America
[3] Department of Applied and Environmental Chemistry, Interdisciplinary Excellence Centre, University of Szeged, Rerrich Béla tér 1, Szeged H-6720, Hungary

E-mail: olli.pitkanen@oulu.fi

Received 8 June 2020, revised 17 August 2020
Accepted for publication 27 August 2020
Published 22 September 2020

**Abstract**

There is ever increasing demand for flexible energy storage devices due to the development of wearable electronics and other small electronic devices. The electrode flexibility is best provided by a special set of nanomaterials, but the required methodology typically consists of multiple steps and are designed just for the specific materials. Here, a facile and scalable method of making flexible and mechanically robust planar supercapacitors with interdigital electrode structure made of commercial carbon nanomaterials and silver nanowires is presented. The capacitor structure is achieved with vacuum filtration through a micropatterned contact mask and finished with simple laser processing steps. A maximum specific capacitance of 4 F $cm^{-3}$ was measured with cyclic voltammetry at scan rate of 5 mV $s^{-1}$. The reliability and charge transfer properties of devices were further investigated with galvanostatic charge-discharge measurements and electrochemical impedance spectroscopy, respectively. Furthermore, mechanical bending tests confirmed the devices have excellent mechanical integrity, and the deformations have no adverse effects on the electrochemical charge-discharge behavior and stability.

Keywords: supercapacitors, vacuum filtration, laser processing, carbon nanotubes, reduced graphene oxide, silver nanowires

Supplementary material for this article is available online

(Some figures may appear in color only in the online journal)

## 1. Introduction

Due to the increasing popularity and market needs of portable electronics, wearable devices and Internet of Things (IoT), there is growing demand for the development of new advanced flexible energy storage devices [1, 2]. Carbon nanomaterials have numerous attractive properties that have been utilized in electrical applications [3]. Their electrical

conductivity, high surface area, chemical stability, light weight as well as mechanical flexibility make them the material of choice in electrodes for electrochemical energy storage, especially for supercapacitors with high power density and excellent cycle stability [4–6]. Among the carbon nanomaterials graphene/reduced graphene oxide (RGO) [7–34], carbon nanotubes (CNTs) [21–27, 35–46], carbon black [7, 8, 47], activated carbon [20, 25, 35, 48], carbon nanofibers [35, 49–51] as well as biomass derived carbon [51–53] have been the most prominent materials for supercapacitor electrodes. Moreover, silver in the form of nanowires [14, 35] and nanoparticles [54] have also been utilized in in the electrode material enhancing the performance of the electrode due to its superior intrinsic electrical conductivity [55].

As the field of flexible electronics grows rapidly, research on flexible supercapacitors have attracted significant attention [14–20, 23–37, 43–48]. Supercapacitors are usually assembled with a stacked configuration, where the two electrodes are wetted by a liquid electrolyte, separated with a spacer and connected by metal current collectors. All-solid-state flexible supercapacitors with a planar interdigital structure however offer a series of advantages, such as low volume, high stability and a control of the electrode design which has a strong influence on the device performance [14]. Most importantly, the devices can be placed in flexible and wearable systems as well as in other portable autonomous electrical circuits that can serve as back-up for uninterruptable power systems, small battery replacements and can be also applied in energy harvester devices to store the scavenged energy.

Vacuum filtration has long been used to make carbon-based films that are then utilized as electrodes. The process itself is facile and quick to produce highly porous carbon films that are either supported by the filter membrane [12–15, 27–29, 37–39] or completely freestanding after removal [7, 20, 23–25, 48]. The films can also be patterned into an interdigital structure by etching the filtered thin film [14] or by multi-step photolithography process [37]. Other reported methods of making carbon-based interdigital electrodes on flexible substrates have been inkjet printing [18, 35], mask-assisted spray coating [18] layer-by-layer assembly [22, 36], film transfer [17, 27, 29–31] and 3D-printing [46]. Moreover, laser processing is one of the most promising method to reduce process steps in microelectronics patterning as it does not require time consuming photolithography steps or vacuum equipment and is capable to process large areas. Laser has been used to process carbonaceous materials, such as graphene and graphene oxide [9–11, 16, 26, 31–33] as well to sinter nanostructured metals [54] and also to enable CNT growth on metal substrates [56].

In this research, we are demonstrating a fast, scalable and straightforward method, in which planar supercapacitor electrodes with interdigital structure are prepared by vacuum filtration through micropatterned contact masks. Though a similar approach have been reported to make interdigital electrodes [27, 29], here no electrode film transfer was needed and a thin layer of silver nanowires (Ag-NWs) is deposited on the top of the carbon film, as a current collector layer to significantly lower the electrode resistance. Carbon nanotubes and RGO were chosen as electrode material due to their well-known properties such as excellent electrical conductivity, large surface and high stability under mechanical stress area which is why they are used in numerous electrochemical energy storage applications [5, 6, 57–59]. The as obtained nanocarbon-Ag capacitor structure is then further processed with a quick laser cleaning of any possible shorts, which is then followed by laser-assisted sintering the Ag-NWs to optimize the conductivity of the collector. By applying a PVA-based electrolyte we obtain solid-state supercapacitor devices that are mechanically robust and suitable for energy storage in wearable and other small electronics demanding flexible power sources.

## 2. Methods

100 mg of graphene oxide (Sigma Aldrich prod. No. 796034) was first mixed in 200 ml of de-ionized (DI) water. 2 g of $NaBH_4$ was then added to the solutions and stirred overnight with a magnetic stirrer at room temperature. The RGO was then filtered on PTFE filter paper (1 $\mu$m pore size), rinsed with DI-water seven times and dried at 70 °C overnight. Suspensions of multi-walled carbon nanotube (MWCNT) (Sigma Aldrich prod. No 773840, 50 mg/L), single wall carbon nanotube (SWCNT) (Sigma Aldrich prod. No 519308, 300 mg $l^{-1}$), RGO (300 mg $l^{-1}$) and Ag-NW (Nanostructured & Amorphous Materials Inc. prod. No #0475NW1 2.5 g $l^{-1}$) were done in isopropyl alcohol (IPA) and sonicated for 30 min. The SWCNT/RGO@IPA suspension were then made by mixing the two suspensions using a 1:1 ratio.

A design of four interdigital capacitor structures of 500 $\mu$m line width and 200 $\mu$m spacing (total electrode area of 0.49 $cm^2$) was cut on biaxially-oriented polyethylene terephthalate (BoPET, thickness of 50 $\mu$m, 47 mm diameter) filter mask by a laser (LPKF Protolaser U3, $\lambda$ = 355 nm). The filter mask is then placed on hydrophilic polyvinylidene fluoride (PVDF, Durapore Millipore GVWP4700, 47 mm diameter, 22 $\mu$m pore size) filter membrane for the vacuum filtering steps. 1 ml of MWCNT@IPA is first applied as a primer layer, which is then followed by 2 ml of SWCNT/RGO@IPA. The filtration assembly is then rinsed with IPA after which 220 $\mu$l of Ag-NW@IPA is applied as current collectors and the structures are left to dry overnight. All suspensions are sonicated for 3 min before applications. The capacitor structures are then trimmed ($P_{avg}$ = 0.9 W, f = 200 kHz) and sintered ($P_{avg}$ = 2 W, f = 120 kHz, off-focus = 12 mm) by a UV-laser (LPKF Protolaser U3, $\lambda$ = 355 nm). The filter membranes were then cut into separate capacitors. The $H_3PO_4$-PVA gel electrolyte was prepared by mixing PVA (Fluka prod. No. 10852, $M_W$ ~ 61 000), and $H_3PO_4$ (SAFC, 85 wt.%) in DI-water in 1:2:10 ratio. The mixture was kept at 80 °C under stirring until a clear solution was obtained. The electrolyte was then cooled down to room temperature, applied on top of the capacitor structures and let to solidify overnight. The ionogel electrolyte was prepared by mixing 110 mg of fumed silica and 3 ml of 1-ethyl-3-methylimidazolium tetrafluoroborate (EMIM-$BF_4$, Sigma Aldrich prod. No. 00768). The mixture was magnetically stirred for 3 h in a nitrogen atmosphere before applying to the capacitor structures.

The electrochemical measurements the capacitors were connected to a potentiostat-galvanostat (Princeton Applied Research VersaSTAT 3) with probes. The electrochemical performance of the capacitors was assessed by cyclic voltammetry (CV), galvanostatic charge-discharge (GDC) and electrochemical impedance spectroscopy (EIS) measurements. The specific volumetric capacitance $C_v$ was calculated from the averages of the integrated current-time hysteresis curves normalized by the electrode volume:

$$C_v = \frac{\int_{U_1}^{U_2} I(U)\,dV}{dU/dt \cdot \Delta U \cdot v} \tag{1}$$

where $I(U)$ is the charging current, $dU/dt$ is the scan rate, $\Delta U$ is the used voltage range between $U_1$ and $U_2$ and $v$ is the volume of the device. The capacitance was calculated from charge-discharge measurements with:

$$C_v = \frac{I}{\Delta U/\Delta t \cdot v} \tag{2}$$

where $I$ is the used current, $\Delta U$ the voltage window, $\Delta t$ is the discharge time and $v$ is the volume of the capacitor. Energy density values of the on-chip devices are obtained from:

$$E_d = \frac{CU^2}{2v} \tag{3}$$

where $C$ is the calculated capacitance from charge-discharge measurements, $U$ is the used voltage range and $v$ is the volume of the device. The power density is calculated using the equation:

$$P_d = \frac{E_d}{\Delta t} \tag{4}$$

where $E_d$ is the calculated energy density from charge-discharge measurements and $\Delta t$ is the discharge time.

X-ray micro-computed tomography analysis was done with Bruker Skyscan 2211 instrument (Projected images were reconstructed using CtVox software). The electrical resistivity measurements were done with a multimeter (Fluke 289 true RMS multimeter) The structure and the materials were assessed with of field emission scanning electron microscope (FESEM, Zeiss Ultra Plus and Zeiss Sigma, light microscope (Olympus BX51 equipped with Colorview imaging system), Raman spectroscope (Horiba Jobin–Yvon LabRAM HR, $\lambda = 488$ nm) and x-ray photoelectron spectroscopy (XPS, Thermo Fisher Scientific Escalab 250 XI system with Al K$\alpha$ x-ray source, 1486.6 eV, data evaluation using Avantage software).

## 3. Results and discussion

The interdigital capacitor structures were prepared using a standard filtration setup (figure 1(a)) combined with a filtration mask. In the process steps (figure 1(b)), the filter mask with the capacitor patterns was first placed on the top of a PVDF filter membrane. The carbon nanomaterial, consisting of SWCNTs and RGO dispersed in IPA, was then filtered through the mask and membrane thus depositing on the open areas of the filtration mask. Using a mixture of CNTs and RGO prevents the graphene sheets from stacking, thus enhancing the effective surface area and performance in a supercapacitor [60]. Next the Ag-NWs were deposited on the top of the carbon nanomaterials to function as a current collector layer. Though the filtration process is simple, quick and effective, the carbon nanomaterial frequently deposited underneath the filter mask because of a slight underflow of the dispersion. This issue was tackled with by depositing a thin layer of MWCNTs as a primer layer. The MWCNTs had a much poorer dispersion in IPA which prevented them from flowing underneath the filtration mask.

Despite the deposited Ag-NWs, the resistivity of the electrodes was still too high ($R_s > 100$ Ω/□) to function properly in a supercapacitor, which was likely caused by the imperfect junctions between the crossing nanowires in the network. To improve the conductivity of the Ag-NW current collector layer, we applied a sintering strategy demonstrated earlier [35, 52]. Here, we used a scanned pulsed laser beam set to a strong off-focus (to increase the effective beam spot size and to avoid ablation of the material) to heat and anneal the crystalline Ag-NWs, which underwent partial melting and fused together at the junctions (figures 2(a) and (b)) thus eliminating the contact resistance and consequently lowering the resistivity of the Ag-NW network (figure 2(c)). In the first laser-assisted sintering cycle, the resistivity decreased over two orders of magnitude from $R_s > 100$ Ω/□ to $R_s \sim 0.3$ Ω/□ after which the subsequent sintering cycles resulted in only very moderate further drop of resistivity. In an attempt to optimize further the conductivity of the collectors, we tested whether thicker Ag-NW networks could have any advantage. The results showed that the resistivity did not significantly improve with higher Ag-NW loadings showing only linear relationship in the analyzed surface loading range between 0.5 mg cm$^{-2}$ and 1.25 mg cm$^{-2}$ with corresponding sheet resistances of 0.28 Ω/□ and 0.12 Ω/□. Based on the results above, in the further part of the work, we applied 100 cycles for laser-assisted sintering of Ag-NW networks with 1.0 mg cm$^{-2}$ surface loading to be used for the electrodes of supercapacitors.

Though the amount of material deposited underneath the filtration mask was significantly reduced by the MWCNT primer layer, there still was an occasional occurrence of carbon material depositing on the interdigital electrode spacings, which was shorting the capacitor structure (figure S1 (available online at stacks.iop.org/NANO/31/495403/mmedia)). The electrode spacings were therefore always cleaned by a laser trimming process using a pulsed UV process laser with a low power adding only one extra phase in the lasering process. As the carbon material effectively absorbs the UV radiation, the trimming process can easily damage the membrane substrate if the power is too high. This was especially prominent when the carbon layer was thick and well absorbing so that the generated heat could partially degrade the PVDF filter underneath [61]. Due to this, and to the apparent material loss, it was not feasible to just filter a uniform layer on carbon material and pattern it by using only laser processing. In this study, the total electrode area of one capacitor was 0.49 cm$^2$ and a total of

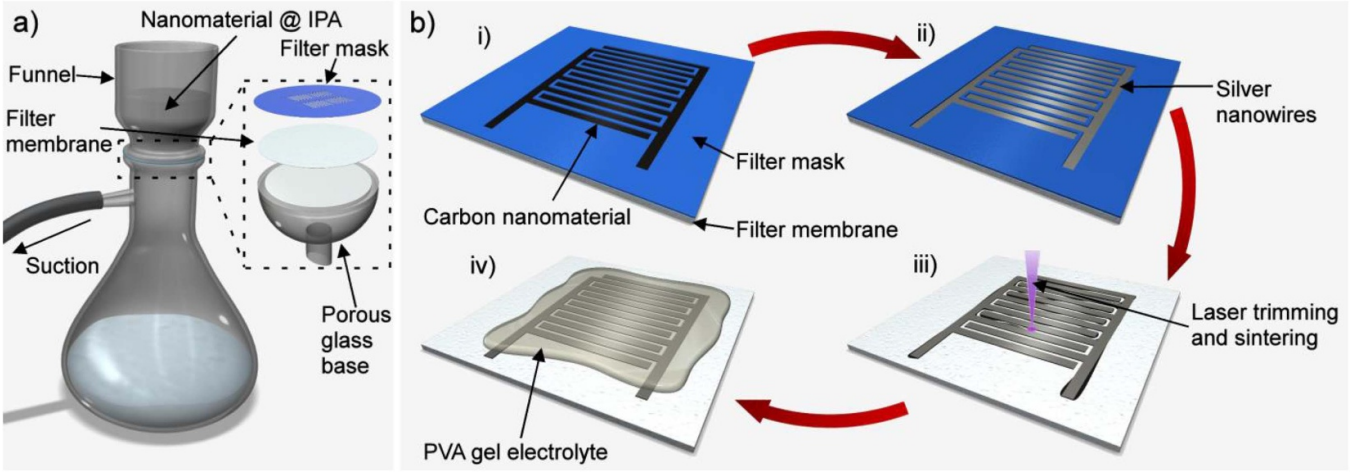


**Figure 1.** (a) Filtration setup. (b) Illustration of the capacitor assembly steps. (i) Carbon nanomaterial deposition on filter membrane through a filtration mask, and (ii) subsequent silver nanowire deposition. (iii) Sintering and trimming of the interdigital electrode pattern by a UV-laser. (iv) Applying PVA gel electrolyte on the electrodes.

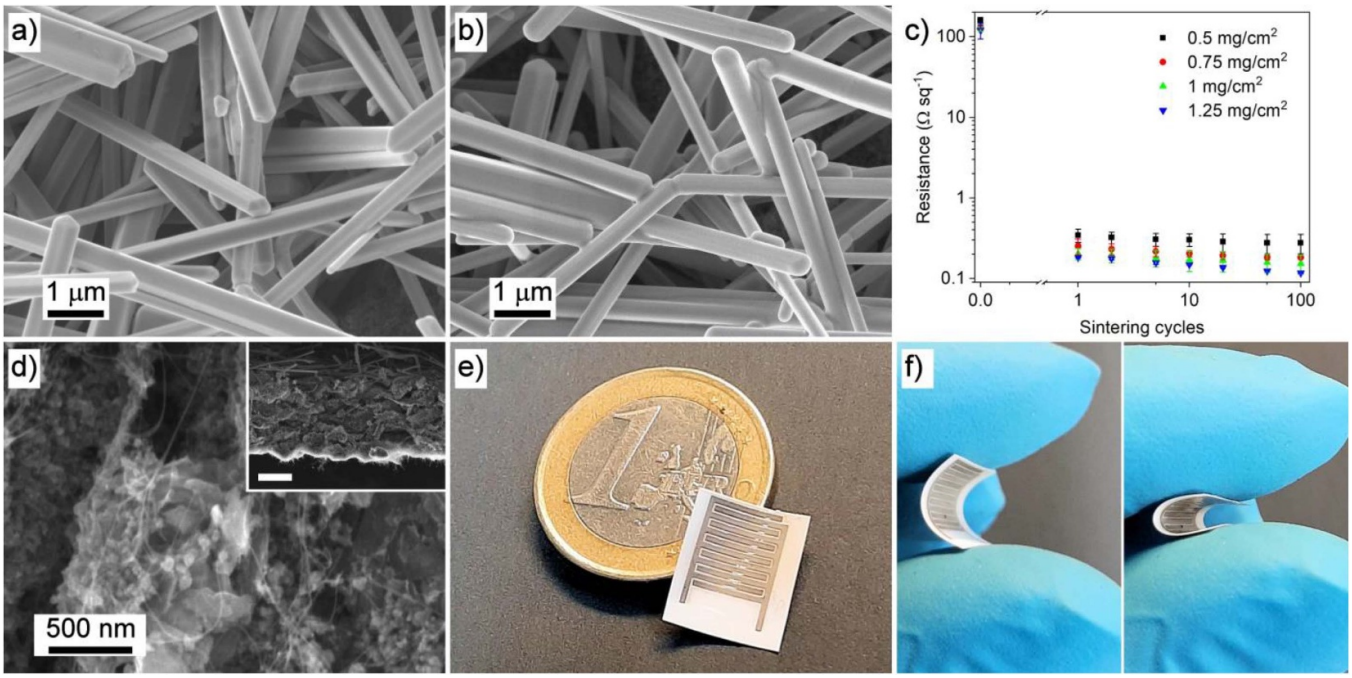


**Figure 2.** (a) SEM image of the pristine silver nanowires on the electrode. (b) SEM image of the silver nanowires after 100 sintering cycles showing the necks of sintered joints at contacts. (c) Effect of laser sintering on the electrode resistance with different Ag-NW loadings. (d) High magnification SEM image of the electrode material taken from the cross-section of the electrode. The inset panel shows a lower magnification cross-section (scale bar is 5 $\mu$m). (e) Optical camera image illustrating the size and the structure of the supercapacitor and (f) flexibility of the device.

650 $\mu$g of carbon material was deposited as electrode material in one capacitor resulting in a film thickness of ~10 $\mu$m (figure 2(d)) which is much thicker than usually reported. However, when investigating the quality of the used commercial carbon nanomaterials, Raman spectroscopy indicate significant concentration of defects in the lattices of both RGO and MWCNT materials [62], which likely reduced the capacity performance (figure S2). XPS analysis of the as-prepared electrode confirm Ag-NWs to be metallic and also show large concentration of carbon-oxygen bonds within the material [63], which is expected (figure S3).

One of the main advantages of this method is that the electrode thickness can be much greater than what is typically reported in planar interdigital capacitor structures made with etching [14, 34], aerosol spraying [18, 33], layer-by-layer assembly [37] or inkjet printing [18, 35]. As a last step the $H_3PO_4$/PVA gel electrolyte was applied on the capacitors and left to dry overnight providing a flexible and robust

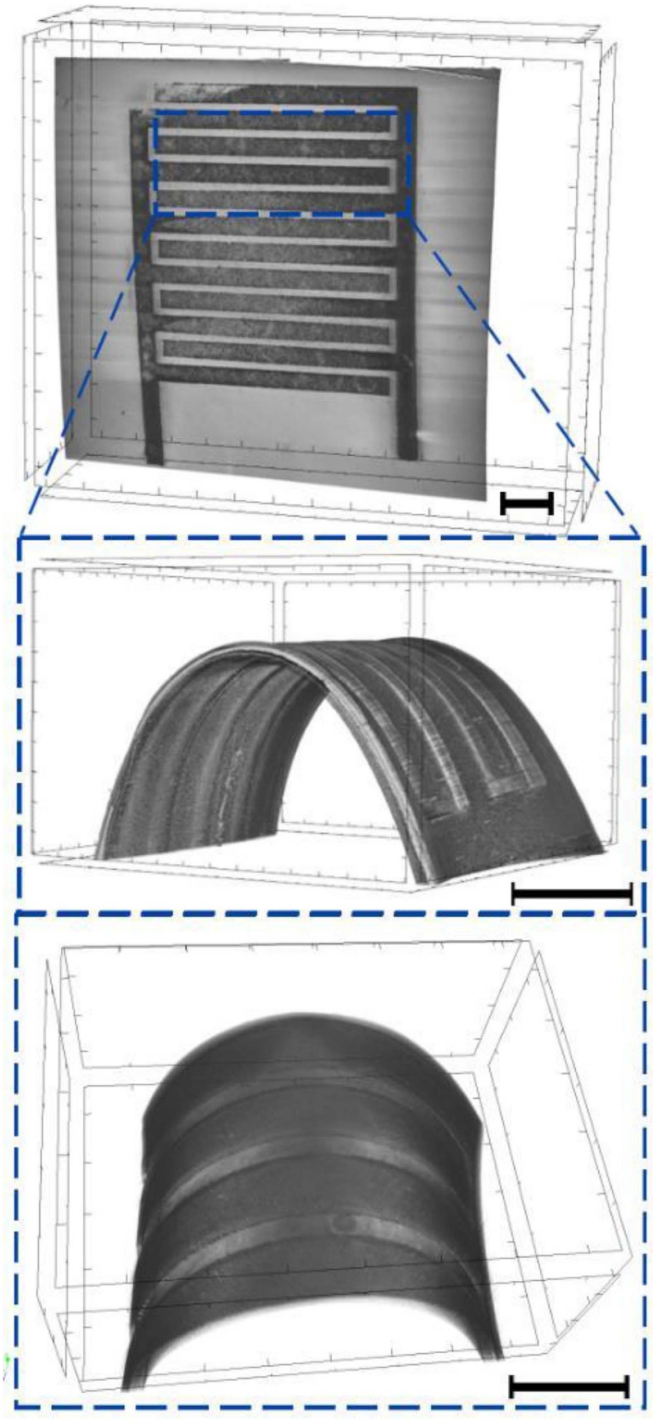

**Figure 3.** X-ray tomography images of the $H_3PO_4$-PVA electrolyte covered electrode under bending. The scalebar is 1 mm.

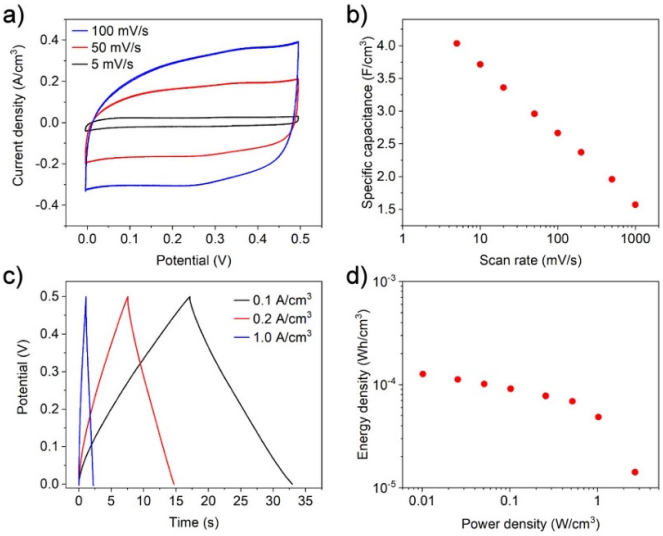


**Figure 4.** (a) Cyclic voltammetry curves of the supercapacitor (b) Corresponding calculated specific capacitances with different scan rates. (c) Charge-discharge curves with different current densities. (d) Ragone plot of energy and power densities.

structure (figures 2(e) and (f)). X-ray micro-computed tomography images of the structures (figure 3) confirm that the electrode films have good mechanical integrity and stay intact upon deformation without any visible delamination observed.

The electrochemical behavior of the supercapacitors was measured in the voltage window between 0 V and 0.5 V (calculation methods and equations are provided in the supporting information). By CV with scanning rates from 5 mV $s^{-1}$ to 1000 mV $s^{-1}$. The CV curves have rounded shape even at slower scan rates (figure 4(a)) indicating ohmic losses in the electrode structure. The highest volumetric capacitance 4 F $cm^{-3}$ was measured at 5 mV $s^{-1}$, and as typical for supercapacitors, decreased at higher scan rates. (figure 4(b)). The GDC curves follow the typical triangular shape (figure 4(c)) and show capacitances very close to those measured with CV (3.7 F $cm^{-3}$ at the lowest current density of 40 mA $cm^{-3}$). Similar to the CV analysis, the measured capacitances dropped at higher current densities due to the increasing voltage drop at the start of the discharge step. The calculated energy and power densities are illustrated in Ragone plot (figure 4(d)). The highest measured energy and power densities were 130 $\mu$Wh $cm^{-3}$ and 2.7 W $cm^{-3}$ respectively as the energy and power performance was significantly limited by the narrow bias window of 0.5 V. The performance of the capacitors is however still well comparable with the state-of-the-art in flexible planar supercapacitors (Supplementary table S1). The methodology reported here have however significant advantages as it is facile, scalable and could be used with multiple different electrode materials.

When using a 0.8 V potential window it was noted that the performance of the capacitor dropped to 85% after 1000 measurement cycles and to 42% after 5000 cycles (figure 5(a)). After 5000 cycles the changes were also clearly visible in the positive electrode that turned dark indicating that the metallic silver have oxidized. Experiments with EMIM-$BF_4$-based gelated ionic liquid (ionogel) that allow for a higher potential window (up to 2 V) enabled higher currents in CV measurements due to the oxidation reaction of the Ag-NWs (figure S4) therefore leading to an even more accelerated performance degradation. This founding was surprising as the Ag-NWs have been previously reported as an electrode material with both $H_3PO_4$/PVA-based electrolytes [64] and with ionogels [35], though it has to be noted that $Ag/Ag^+$ has a redox potential of 0.799 V vs normal hydrogen electrode which also

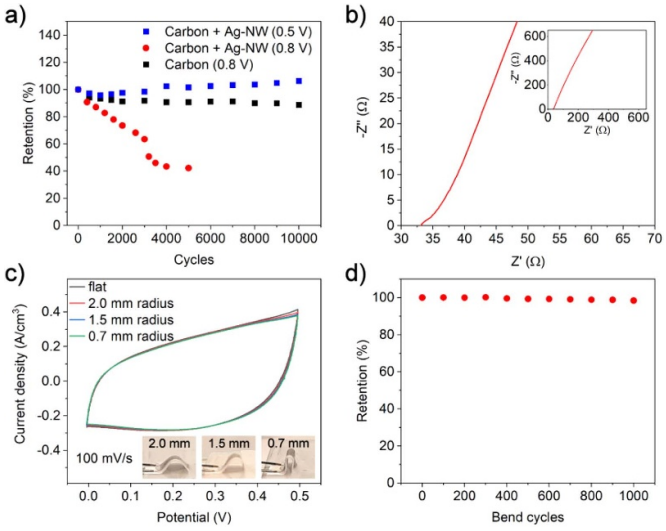


**Figure 5.** (a) Retention of the capacitance with different with and without silver nanowires in 0.5 V and 0.8 V potential ranges. (b) Nyquist diagram according to EIS measurement on the supercapacitor. (c) Cyclic voltammetry curves under different bending conditions. (d) Retention of capacitance as a function of repeated bending cycles.

decreases according to the size of the nanoparticle [65]. One possible explanation could be that the role of the Ag-NWs was not as significant as in this research as a current collector and therefore the degradation did not significantly affect the performance. Without using the Ag-NWs the capacitive performance was still 89% after 10 000 cycles indicating that there still were some irreversible chemical reactions occurring on the carbon material surfaces likely be due to impurities. The capacitor performance without the Ag-NWs as a current collector was however rather poor as the series resistance was almost two orders of magnitude higher (figure S5). With 0.5 V potential range the capacitive performance dropped initially to 96% after the first 1000 cycles after which the performance slowly improved and was 106% of the original performance after 10 000 cycles indicating a good material reliability when using a 0.5 V potential range. No visible aggregation of the electrode material was seen after the retention tests. From EIS measurements the series resistance was evaluated to be ~33 Ω (figure 5(b)). The Nyquist diagram does not show a clear half-circle indicating low charge transfer resistance. As the resistance of the electrode after Ag-NW sintering was ~0.1 Ω/□ the resistivity is likely due to the carbon materials used in this research. This was also indicated by the lower series resistance of capacitors made with thinner electrode material layers.

Mechanical bending tests conjunction with CV measurements were conducted to assess the reliability of the flexible capacitors. The capacitors exhibited excellent stability. Even with 0.7 mm bending radius, the shape of the CV curve does not change, and the overall capacitance is only 1% lower (figure 5(c)). The same behavior is also visible with retention tests that show the performance was still 98% of the original value after 1000 bending cycles with ~1 mm bending radius (figure 5(d)) indicating excellent overall stability under mechanical stress as expected from the x-ray topology analysis.

## 4. Summary and conclusions

Here we have demonstrated a fast and easily up and down scalable method of producing interdigital supercapacitor structures by straightforward filtering steps using commercially available materials such as SWCNTs and MWCNTs, RGO and Ag-NWs on PVDF filter substrates. We have shown that laser-assisted sintering of Ag-NWs deposited on nanostructured carbon-based interdigital porous electrode films allow for the fabrication of highly conductive current collectors of high performance flexible planar supercapacitors. Using $H_3PO_4$/PVA electrolytes, volumetric capacitances of up to 4 F cm$^{-3}$ were achieved. According to our study, the suitability of Ag-NWs as an electrode material in supercapacitors is limited to a small electrochemical window due to the oxidation of silver above 0.5 V.

While our work shows a simple method to achieving planar flexible capacitor devices, we envisage a number of possibilities that could improve the overall performance of the devices. For instance, the collector may be optimized further by replacing silver with gold (or with gold coated core–shell nanowires) to expand the voltage window. Another possible method to decrease the series resistance could be to use the filtering mask also as a shadow mask for physical vapor deposition of a metal thin film for the current collector. This would of course demand very careful work not to move the mask between the steps. Moreover, the performance could be also significantly improved by utilizing nanostructured carbons with higher specific surface area and conductivity than those applied in this study. It shall be also noted here, that the capacitance of the devices may be increased further significantly by adding pseudocapacitive materials such as oxides of manganese or ruthenium on the electrodes [40, 66, 67].

## Acknowledgments

The financial support received partly from EU Interreg Nord—Lapin liitto (project Transparent, conducting and flexible films for electrodes), University of Oulu (projects Entity and PoC: Ultra-low permittivity and loss porous nanocomposites for future 6G telecommunication), Academy of Finland (project: Nigella), Hungarian National Research, Development and Innovation Office through the projects GINOP-2.3.2-15-2016-00013 and GINOP-2.3.3-15-2016-00010, and the Ministry of Human Capacities, Hungary, Grant No. 20391-3/2018/FEKUSTRAT is acknowledged. O.P and D.S. are thankful for the Ulla Tuominen foundation and János Bolyai Research Scholarship of the Hungarian Academy of Sciences, respectively. We acknowledge the technical help received from the Micro- and Nanotechnology Center, University of Oulu.

## ORCID iDs

Olli Pitkänen https://orcid.org/0000-0003-2870-3229
Ákos Kukovecz https://orcid.org/0000-0003-0716-9557
Robert Vajtai https://orcid.org/0000-0002-3942-8827

Krisztian Kordas https://orcid.org/0000-0002-7331-1278

## References


[1] Gür T M 2018 Review of electrical energy storage technologies, materials and systems: challenges and prospects for large-scale grid storage *Energy Environ. Sci.* **11** 2696

[2] Noori A, El-Kady M F, Rahmanifar M S, Kaner R B and Mousavi M F 2019 Towards establishing standard performance metrics for batteries, supercapacitors and beyond *Chem. Soc. Rev.* **48** 1272

[3] Jariwala D, Sangwan V K, Lauhon L J, Marks T J and Hersam M C 2013 Carbon nanomaterials for electronics, optoelectronics, photovoltaics, and sensing *Chem. Soc. Rev.* **42** 2824

[4] Yu M and Feng X 2019 Thin-film electrode-based supercapacitors *Joule* **3** 338

[5] Dubey R and Guruviah V 2019 Review of carbon-based electrode materials for supercapacitor energy storage *Ionics* **25** 1419

[6] Poonam , Sharma K, Arora A and Tripathi S K 2019 Review of supercapacitors: materials and devices *J. Energy Storage* **21** 801

[7] Wang Y, Chen J, Cao J, Liu Y, Zhou Y, Ouyang J-H and Jia D 2014 Graphene/carbon black hybrid film for flexible and high rate performance supercapacitor *J. Power Sources* **271** 269

[8] Yan J, Wei T, Shao B, Ma F, Fan Z, Zhang M, Zheng C, Shang Y, Qian W and Wei F 2010 Electrochemical properties of graphene nanosheet/carbon black composites as electrodes for supercapacitors *Carbon* **48** 1731

[9] Gao W *et al* 2011 Direct laser writing of micro-supercapacitors on hydrated graphite oxide films *Nat. Nanotechnol.* **6** 496

[10] Lamberti A, Perrucci F, Caprioli M, Serrapede M, Fontana M, Bianco S, Ferrero S and Tresso E 2017 New insights on laser-induced graphene electrodes for flexible supercapacitors: tunable morphology and physical properties *Nanotechnology* **28** 174002

[11] Lin J, Peng Z, Liu Y, Ruiz-Zepeda F, Ye R, Samuel E L G, Yacaman M J, Yakobson B I and Tour J M 2014 Laser-induced porous graphene films from commercial polymers *Nat. Commun.* **5** 5714

[12] Hamra A A B, Lim H N, Chee W K and Huang N M 2016 Electro-exfoliating graphene from graphite for direct fabrication of supercapacitor *Appl. Surf. Sci.* **360** 213

[13] Zhang S, Li Y and Pan N 2012 Graphene based supercapacitor fabricated by vacuum filtration deposition *J. Power Sources* **206** 476

[14] Liu W, Lu C, Wang X, Tay R Y and Tay B K 2015 High-performance microsupercapacitors based on two-dimensional graphene/manganese dioxide/silver nanowire ternary hybrid film *ACS Nano* **9** 1528

[15] Eda G, Fanchini G and Chhowalla M 2008 Large-area ultrathin films of reduced graphene oxide as a transparent and flexible electronic material *Nat. Nanotechnol.* **3** 270

[16] El-Kady M F, Strong V, Dubin S and Kaner R B 2012 Laser scribing of high-performance and flexible graphene-based electrochemical capacitors *Science* **335** 1326

[17] Peng L, Peng X, Liu B, Wu C, Xie Y and Yu G 2013 Ultrathin two-dimensional $MnO_2$/graphene hybrid nanostructures for high-performance, flexible planar supercapacitors *Nano Lett.* **13** 2151

[18] Liu Z, Wu Z-S, Yang S, Dong R, Feng X and Müllen K 2016 Ultraflexible in-plane micro-supercapacitors by direct printing of solution-processable electrochemically exfoliated graphene *Adv. Mater.* **28** 2217

[19] Cong H-P, Ren X-C, Wang P and Yu S-H 2013 Flexible graphene–polyaniline composite paper for high-performance supercapacitor *Energy Environ. Sci.* **6** 1185

[20] Huang Z, Guo H and Zhang C 2019 Assembly of 2D graphene sheets and 3D carbon nanospheres into flexible composite electrodes for high-performance supercapacitors *Compos. Commun.* **12** 117

[21] Cheng Q, Tang J, Ma J, Zhang H, Shinya N and Qin L-C 2011 Graphene and carbon nanotube composite electrodes for supercapacitors with ultra-high energy density *PCCP* **13** 17615

[22] Pansri S and Noothongkaew S 2019 MWCNTs/r-GO hybrid films fabricated by layer by layer assembly for supercapacitor electrodes *J. Energy Storage* **22** 153

[23] Yang Z-G, Liu -N-N, Dong S, Tian F-S, Gao Y-P and Hou Z-Q 2018 Supercapacitors based on free-standing reduced graphene oxides/carbon nanotubes hybrid films *SN Appl. Sci.* **1** 47

[24] He J, Yang D, Li H, Cao X, Kang L, He X, Jiang R, Sun J, Lei Z and Liu Z-H 2018 $Mn_3O_4$/RGO/SWCNT hybrid film for all-solid-state flexible supercapacitor with high energy density *Electrochim. Acta* **283** 174

[25] Li X, Tang Y, Song J, Yang W, Wang M, Zhu C, Zhao W, Zheng J and Lin Y 2018 Self-supporting activated carbon/carbon nanotube/reduced graphene oxide flexible electrode for high performance supercapacitor *Carbon* **129** 236

[26] Mao X, Xu J, He X, Yang W, Yang Y, Xu L, Zhao Y and Zhou Y 2018 All-solid-state flexible microsupercapacitors based on reduced graphene oxide/multi-walled carbon nanotube composite electrodes *Appl. Surf. Sci.* **435** 1228

[27] Xiao H, Wu Z-S, Zhou F, Zheng S, Sui D, Chen Y and Bao X 2018 Stretchable tandem micro-supercapacitors with high voltage output and exceptional mechanical robustness *Energy Storage Mater.* **13** 233

[28] Wang X, Wang R, Zhao Z, Bi S and Niu Z 2019 Controllable spatial engineering of flexible all-in-one graphene-based supercapacitors with various architectures *Energy Storage Mater.* **23** 269

[29] Xiao H, Wu Z-S, Chen L, Zhou F, Zheng S, Ren W, Cheng H-M and Bao X 2017 One-step device fabrication of phosphorene and graphene interdigital micro-supercapacitors with high energy density *ACS Nano* **11** 7284

[30] Shi Q, Xiang Y, Ji G, Wang D, Wang X, Xu R, Jiang L, Yu Y and Zhao J 2019 Flexible planar-integrated micro-supercapacitors from electrochemically exfoliated graphene as advanced electrodes prepared by flash foam–assisted stamp technique on paper *Energy Technol.* **7** 1900664

[31] Chen Y, Xu B, Xu J, Wen J, Hua T and Kan C-W 2019 Graphene-based in-planar supercapacitors by a novel laser-scribing, *in-situ* reduction and transfer-printed method on flexible substrates *J. Power Sources* **420** 82

[32] El-Kady M F and Kaner R B 2013 Scalable fabrication of high-power graphene micro-supercapacitors for flexible and on-chip energy storage *Nat. Commun.* **4** 1475

[33] Shao Y, Li J, Li Y, Wang H, Zhang Q and Kaner R B 2017 Flexible quasi-solid-state planar micro-supercapacitor based on cellular graphene films *Mater. Horiz.* **4** 1145

[34] Wu Z S, Parvez K, Feng X and Müllen K 2013 Graphene-based in-plane micro-supercapacitors with high power and energy densities *Nat. Commun.* **4** 2487

[35] Choi K-H, Yoo J, Lee C K and Lee S-Y 2016 All-inkjet-printed, solid-state flexible supercapacitors on paper *Energy Environ. Sci.* **9** 2812

[36] Lee G, Kim D, Yun J, Ko Y, Cho J and Ha J S 2014 High-performance all-solid-state flexible

micro-supercapacitor arrays with layer-by-layer assembled MWNT/MnOx nanocomposite electrodes *Nanoscale* **6** 9655
[37] Chen Y-T, Ma C-W, Chang C-M and Yang Y-J 2018 Micromachined planar supercapacitor with interdigital buckypaper electrodes *Micromachines* **9** 242
[38] Ervin M H, Miller B S, Hanrahan B, Mailly B and Palacios T 2012 A comparison of single-wall carbon nanotube electrochemical capacitor electrode fabrication methods *Electrochim. Acta* **65** 37
[39] Rautio A-R, Pitkänen O, Järvinen T, Samikannu A, Halonen N, Mohl M, Mikkola J-P and Kordas K 2015 Electric double-layer capacitors based on multiwalled carbon nanotubes: can nanostructuring of the nanotubes enhance performance? *J. Phys. Chem.* C **119** 3538
[40] Pitkänen O *et al* 2017 On-chip integrated vertically aligned carbon nanotube based super- and pseudocapacitors *Sci. Rep.* **7** 16594
[41] Futaba D N, Hata K, Yamada T, Hiraoka T, Hayamizu Y, Kakudate Y, Tanaike O, Hatori H, Yumura M and Iijima S 2006 Shape-engineerable and highly densely packed single-walled carbon nanotubes and their application as super-capacitor electrodes *Nat. Mater.* **5** 987
[42] Pitkänen O, Lorite G S, Shi G, Rautio A R, Uusimäki A, Vajtai R, Tóth G and Kordás K 2015 The effect of Al buffer layer on the catalytic synthesis of carbon nanotube forests *Top. Catal.* **58** 1112
[43] Kang Y J, Chung H, Han C-H and Kim W 2012 All-solid-state flexible supercapacitors based on papers coated with carbon nanotubes and ionic-liquid-based gel electrolytes *Nanotechnology* **23** 065401
[44] Hsia B, Marschewski J, Wang S, In J B, Carraro C, Poulikakos D, Grigoropoulos C P and Maboudian R 2014 Highly flexible, all solid-state micro-supercapacitors from vertically aligned carbon nanotubes *Nanotechnology* **25** 055401
[45] Kanninen P, Luong N D, Sinh L H, Anoshkin I V, Tsapenko A, Seppälä J, Nasibulin A G and Kallio T 2016 Transparent and flexible high-performance supercapacitors based on single-walled carbon nanotube films *Nanotechnology* **27** 235403
[46] Yu W, Zhou H, Li B Q and Ding S 2017 3D printing of carbon nanotubes-based microsupercapacitors *ACS Appl. Mater. Interfaces* **9** 4597
[47] Kossyrev P 2012 Carbon black supercapacitors employing thin electrodes *J. Power Sources* **201** 347
[48] Chen J, Fang K, Chen Q, Xu J and Wong C-P 2018 Integrated paper electrodes derived from cotton stalks for high-performance flexible supercapacitors *Nano Energy* **53** 337
[49] Kim C and Yang K S 2003 Electrochemical properties of carbon nanofiber web as an electrode for supercapacitor prepared by electrospinning *Appl. Phys. Lett.* **83** 1216
[50] El-Shafei M H, Hassanin A H, Shaalan N M, Sharshar T and El-Moneim A A 2020 Free-standing interconnected carbon nanofiber electrodes: new structural designs for supercapacitor application *Nanotechnology* **31** 185403
[51] Wei J, Geng S, Pitkänen O, Järvinen T, Kordas K and Oksman K 2020 Green carbon nanofiber networks for advanced energy storage *ACS Appl. Energy Mater.* **3** 3530
[52] Li H, Cao L, Wang F, Duan G, Xu W, Mei C, Zhang G, Liu K, Yang M and Jiang S 2020 Fatsia Japonica-derived hierarchical porous carbon for supercapacitors with high energy density and long cycle life *Frontiers Chem.* **8** 89
[53] Wang F, Chen L, Li H, Duan G, He S, Zhang L, Zhang G, Zhou Z and Jiang S 2020 N-doped honeycomb-like porous carbon towards high-performance supercapacitor *Chin. Chem. Lett.* **31** 1986
[54] Lee J, Seok J Y, Son S, Yang M and Kang B 2017 High-energy, flexible micro-supercapacitors by one-step laser fabrication of a self-generated nanoporous metal/oxide electrode *J. Mater. Chem.* A **5** 24585
[55] Chen Y, Pang L, Li Y, Luo H, Duan G, Mei C, Xu W, Zhou W, Liu K and Jiang S 2020 Ultra-thin and highly flexible cellulose nanofiber/silver nanowire conductive paper for effective electromagnetic interference shielding *Composites* A **135** 105960
[56] Pitkänen O, Hart A H C, Vajtai R, Ajayan P M and Kordas K 2018 Maskless direct growth of carbon nanotube micropatterns on metallic substrates *Carbon* **140** 610
[57] Yu J, Liu S, Duan G, Fang H and Hou H 2020 Dense and thin coating of gel polymer electrolyte on sulfur cathode toward high performance Li-sulfur battery *Compos. Commun.* **19** 239
[58] Xu W, Ding Y, Yu Y, Jiang S, Chen L and Hou H 2017 Highly foldable PANi@CNTs/PU dielectric composites toward thin-film capacitor application *Mater. Lett.* **192** 25
[59] Yang H, Liu S, Cao L, Jiang S and Hou H 2018 Superlithiation of non-conductive polyimide toward high-performance lithium-ion batteries *J. Mater. Chem.* A **6** 21216
[60] Wang Y, Wu Y, Huang Y, Zhang F, Yang X, Ma Y and Chen Y 2011 Preventing graphene sheets from restacking for high-capacitance performance *J. Phys. Chem.* C **115** 23192
[61] Lee S, Bordatchev E V and Zeman M J F 2008 Femtosecond laser micromachining of polyvinylidene fluoride (PVDF) based piezo films *J. Micromech. Microeng.* **18** 045011
[62] Dresselhaus M S, Jorio A, Hofmann M, Dresselhaus G and Saito R 2010 Perspectives on carbon nanotubes and graphene Raman spectroscopy *Nano Lett.* **10** 751
[63] NIST X-ray photoelectron spectroscopy database (https://srdata.nist.gov/xps/doi:10.18434/T4T88K)
[64] Liu X, Li D, Chen X, Lai W-Y and Huang W 2018 Highly transparent and flexible all-solid-state supercapacitors based on ultralong silver nanowire conductive networks *ACS Appl. Mater. Interfaces* **10** 32536
[65] Ivanova O S and Zamborini F P 2010 Size-dependent electrochemical oxidation of silver nanoparticles *J. Am. Chem. Soc.* **132** 70
[66] Augustyn V, Simon P and Dunn B 2014 Pseudocapacitive oxide materials for high-rate electrochemical energy storage *Energy Environ. Sci.* **7** 1597
[67] Simon P and Gogotsi Y 2008 Materials for electrochemical capacitors *Nat. Mater.* **7** 845